

Gecko-Inspired Dry Adhesive for Robotic Applications

Jing Yu, Sathya Chary, Saurabh Das, John Tamelier, Noshir S. Pesika, Kimberly L. Turner,* and Jacob N. Israelachvili*

Most geckos can rapidly attach and detach from almost any kind of surface. This ability is attributed to the hierarchical structure of their feet (involving toe pads, setal arrays, and spatulae), and how they are moved (articulated) to generate strong adhesion and friction forces on gripping that rapidly relax on releasing. Inspired by the gecko's bioadhesive system, various structured surfaces have been fabricated suitable for robotic applications. In this study, x - y - z asymmetric, micrometer-sized rectangular flaps composed of polydimethylsiloxane (PDMS) were fabricated using massively parallel micro-electromechanical systems (MEMS) techniques with the intention of creating directionally responsive, high-to-low frictional-adhesion toe pads exhibiting properties similar to those found in geckos. Using a surface forces apparatus (SFA), the friction and adhesion forces of both vertical (symmetric) and angled/tilted (x - y - z asymmetric) microflaps under various loading, unloading and shearing conditions were investigated. It was found that the anisotropic structure of tilted microflaps gives very different adhesion and tribological forces when articulated along different x - y - z directions: high friction and adhesion forces when articulated in the y - z plane along the tilt (+ y) direction, which is also the direction of motion, and weak friction and adhesion forces when articulated against the tilt ($-y$) direction. These results demonstrate that asymmetric angled structures, as occur in geckos, are required to enable the gecko to optimize the requirements of high friction and adhesion on gripping, and low frictional-adhesion on releasing. These properties are intimately coupled to a (also optimum) articulation mechanism. We discuss how both of these features can be simultaneously optimized in the design of robotic systems that can mimic the gecko adhesive system.

1. Introduction

Geckos have a remarkable climbing ability by using a vast array of multi-scale hierarchical structures. The hierarchical structure of the feet of Tokay geckos is shown in Figure 1. Each gecko foot has 5 toes; each toe has about 20 arrays (lamellae) of micrometer-scale hair (setae), with each seta being ~ 5 μm in diameter and approximately 110 μm in length on average. Each seta splits into 100–1000 nano-scale spatula, of 200 nm length and width at the tip, forming the fine structure of the gecko adhesive system.^[1] These spatulae, by conforming to both micro- and nano-scale asperities, achieve a large true area of contact, so that geckos can adhere to different surfaces via the weak van der Waals force together with other types of noncovalent forces such as capillary forces.^[2,3] Recent experiments demonstrate that under certain environmental conditions the gecko adhesive pads, by changing their hydrophobicity under humid conditions, also have the ability to exploit environmental conditions to maximize their adhesion and stabilize their friction forces.^[3,4]

The van der Waals force is weak for a single small contact such as a spatula, but this force can be substantial when summed over the large contact area created by all the available spatulae. Measurements on the gecko have reported that the surface area of the two front feet is able to generate a total

friction force of ~ 20 N, an average shear force per seta of ~ 6.2 μN .^[5] Tests on single setae showed that the shear force could reach as high as 194 μN .^[6] Small scale tests often give high forces that are often not attainable in large scale tests because of the inability of all the spatulae to make sufficient contact with other surfaces, even on ones that are smooth.^[7] This problem is amplified for the animal in its natural environment where surfaces, such as bark and rock, can contain varying degrees of roughness. The effect of roughness on the adhesion of elastic plates has been investigated theoretically.^[8,9] However, there has been no systematic study of the effect of roughness on friction.

Theoretical approaches have also shown that both the van der Waals adhesion and the friction forces of flexible, tilted, and optimally spaced setal stalks or synthetic pillars are high enough to support a human being on rough surfaces such as

J. Yu, S. Das, Prof. J. N. Israelachvili
Department of Chemical Engineering
University of California
Santa Barbara, CA 93106, USA
E-mail: jacob@engineering.ucsb.edu
S. Chary, J. Tamelier, Prof. K. L. Turner
Department of Mechanical Engineering
University of California
Santa Barbara, CA 93106, USA
E-mail: turner@engineering.ucsb.edu
Prof. N. S. Pesika
Department of Chemical Engineering
Tulane University
New Orleans, LA 70118, USA

DOI: 10.1002/adfm.201100493

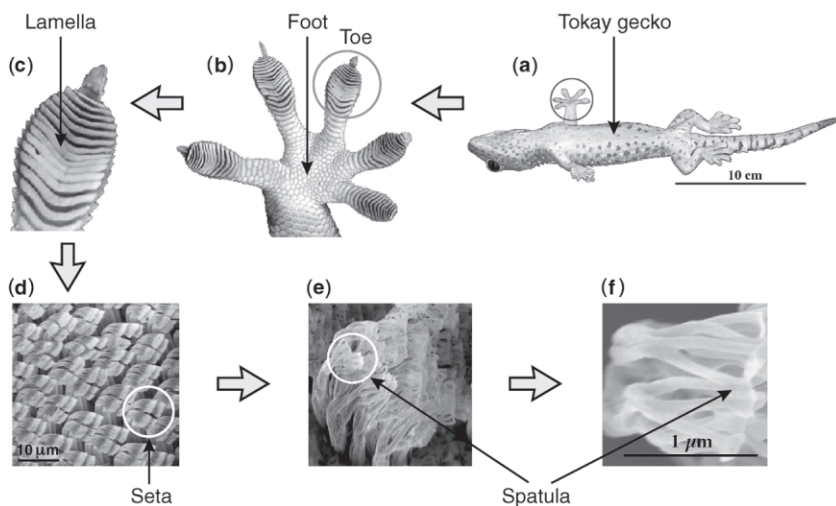


Figure 1. Hierarchical structures of a Tokay gecko. a) Optical image of a Tokay gecko at rest. b) A gecko foot. c) A gecko toe. d) Scanning electron microscope images of a setal array, e) the spatula pads, and f) a magnified view of a spatula pad. Reproduced with permission.^[12] Copyright National Academy of Sciences of the USA, 2006.

ceilings (adhesion) and walls (friction) with an estimated effective area of 230 cm², close to the total area of a human being's hands and feet.^[10,11]

Another key feature of the gecko adhesion system is the significant high reversible adhesion and friction (i.e., rapid sticking and unsticking, as occurs during rapid running on walls or ceilings). The fast detachment is achieved by the highly specialized peeling mechanism of the toes.^[12,13] Further, recent experimental and theoretical findings have demonstrated that the setae on the gecko's feet are angled so as to naturally exhibit anisotropy in their adhesion and friction forces when engaged and displaced along opposing directions.^[13,14] The setae are ~5 μm wide and ~110 μm in length, and start at an angle of 45° with respect to the skin. Upon attachment (in the shear gripping motion), the setae bend down as the toes grip the substrate and the setae are pulled closer to the surface, which gives high adhesion and friction. To detach (in the shear releasing motion), the toes peel away from the surface, and the setae bend back to reduce both adhesion and friction forces.

The extraordinary climbing ability of geckos has inspired extensive studies in designing dry, responsive adhesive systems and robots. Various kinds of patterned surfaces of different shapes and materials with micro- to nano-scale structures have been fabricated.^[15–19] These structures mainly focus on enhancing adhesion properties. While some other attempts focus on both friction and adhesion, they commonly use cylindrical micro-fibers, which only provide a line contact with the adhering surface when sheared, limiting the real surface area of contact for van der Waals forces.^[20–23] The classic Johnson–Kendall–Roberts (JKR) theory has been extensively applied to various bio-adhesion systems.^[2,24,25] The adhesion force between a sphere of radius r and a plane is given by

$$F_{ad} = \frac{3}{2} \pi r W_{12} \quad (1)$$

Where $W_{12} = \gamma_1 + \gamma_2 - \gamma_{12}$ is the thermodynamic work of adhesion, and γ_1 , γ_2 , and γ_{12} are the surface and interfacial energies of two interacting surfaces.

The lateral force or the friction force is even more important when the gecko climbs on walls. A general equation that describes the friction force, F_{\parallel} , between two adhesive surfaces is

$$F_{\parallel} = \mu F_{\perp} + S_c A_{real} \quad (2)$$

where F_{\perp} is the normal load, μ is the friction coefficient, S_c is the shear strength, and A_{real} is the real contact area. The first term of Equation 2 is Amontons' law for non-adhering surfaces, and it dominates the friction at high loads. The second term is the adhesion-dependent contribution, which is proportional to the 'real' molecular contact area. It exists at zero and even negative loads so long as two surfaces are still in contact over a finite area. For the gecko adhesion system, the load contribution is very small, and the adhesion contribution therefore dominates the friction force.

In this study, vertical (Figure 2a) and pre-angled (Figure 2b) PDMS microflap structures mimicking the angled setae structure of the gecko feet were manufactured using micro-fabrication techniques. We have developed a new SFA (surface forces apparatus) 3D force displacement attachment to investigate the adhesion and friction properties of both microflaps. We found that the tilted flap-structure could provide strong frictional adhesion that mimics the gecko adhesion system.

2. Experimental Section

2.1. Fabrication

Large arrays of both vertical and angled microflap structures have been fabricated using microfabrication techniques. To

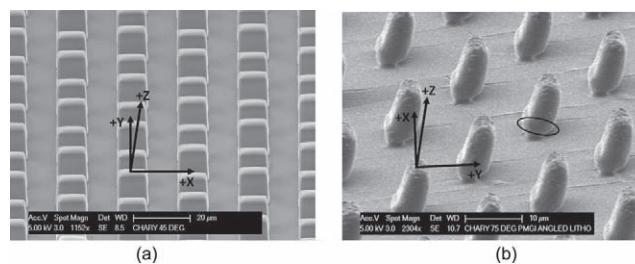


Figure 2. Scanning electron microscope (SEM) images of a) vertical PDMS flaps, b) -20° angled PDMS flaps of 10.2 μm height, with a bulged out region due to undercut in PMGI negative mold (marked by the oval). In all images, the $\pm x$ directions are the directions parallel to the long edge of the flaps; the $+y$ direction is the direction of tilt of the flaps, also the "gripping" direction, and the direction of motion; the $-y$ direction is the "releasing" direction; $-z$ is the (vertical) loading direction, and $+z$ is the unloading direction. Articulation of the feet (toe pads and setae) occur in the y - z plane.

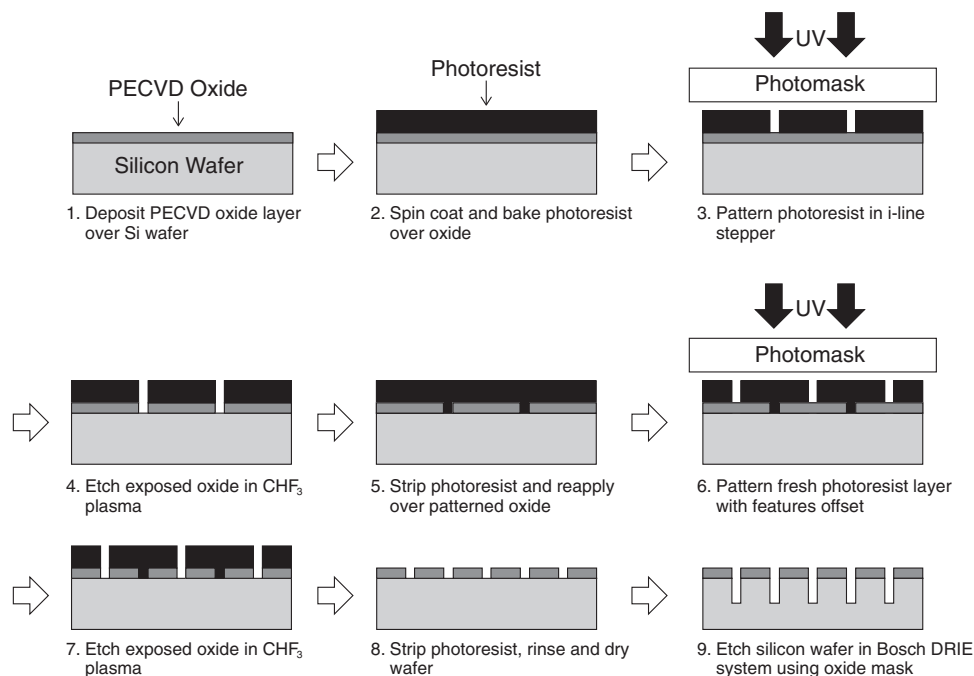


Figure 3. Schematic of the microfabrication process used to fabricate a negative silicon mold for vertical (symmetric) PDMS microflaps. A two stage lithography process was used to increase the area coverage of the flaps.

to fabricate the vertical flaps, a negative silicon mold was prepared by first defining the flap lateral dimensions by lithography in an i-line stepper (GCA 6300, Refurbished by RTS Technologies, Doylestown, PA), and then etching into a single crystal silicon wafer up to the desired depth using the Bosch deep reactive ion etching (DRIE) process.

To increase (double) the areal density of the flap structures using the same lithographic mask, this process was slightly modified (Figure 3). A 0.5 μm thick layer of silicon oxide was deposited on a clean silicon wafer using a plasma-enhanced chemical vapor deposition (PECVD) system. An approximately 1.0 μm thick layer of AZ 5214, an image reversal photoresist (AZ Electronic Materials, Branchburg, NJ), was spin coated over the wafer, and slots for flaps, 4 μm by 10 μm in lateral dimension, were defined by lithography. The oxide layer exposed in these slots was etched away in a CHF_3 plasma using an inductively coupled plasma reactive ion etching system (ICP-RIE). The photoresist layer was now stripped away using Microposit 1165 photoresist stripping solution. A fresh coat of AZ 5214 photoresist was applied to the cleaned and dried wafer and a second set of slots for flaps was subsequently defined using lithography, the second set of flaps being offset symmetrically from the first in the interstitial spaces. The exposed oxide layer was again etched away using the same ICP etch process. After stripping off the photoresist from the second lithography step, the cleaned and dried wafer was ready for the silicon etch step in the Bosch DRIE system, with the patterned oxide layer acting as an effective etch mask. The micro-scale rectangular slots were vertically etched to a depth of 15 μm in the Bosch DRIE system.

The negative mold fabricated by this method was then prepared for PDMS molding by vapor depositing a silane layer.

PDMS (Sylgard 184, Dow Corning, Midland, MI) was mixed in a 10:1 ratio by weight with a crosslinker, and poured over the negative mold. This was degassed and then cured at 100 $^\circ\text{C}$ for 10 min in a convection oven to fully cure the PDMS. The two materials were then separated by carefully peeling off the cured PDMS, resulting in cm-scale PDMS samples with microflaps and a silicon mold that could be reused.

Fabrication of angled flaps necessitated development of a different microfabrication technique (Figure 4). To fabricate large arrays of angled microflap structures over cm-scale areas, an angled exposure for lithography was used, requiring the use of a non-reflective glass substrate wafer. A clean and dry glass wafer was coated with a photoresist bilayer – first with a ~ 10 μm thick layer of polymethylglutarimide (PMGI) positive tone photoresist (PMGI SF-15, MicroChem Corp., Newton, MA), and then with a top layer of AZ 5214 image reversal photoresist approximately 1.4 μm thick. The desired thickness for the PMGI SF-15 layer was obtained by applying two coats of the photoresist at a low spin speed of 1000 rpm, with a short soft bake of 1 min at 200 $^\circ\text{C}$ between the two coats.

The two photoresist materials are sensitive to different wavelengths of UV light, PMGI to the deep UV range of wavelengths between 200 and 260 nm, and AZ 5214 to the i-line UV wavelength of 365 nm. The flap lateral dimensions were defined in the i-line lithography step used to pattern the AZ 5214 imaging resist layer on top. After developing this resist in AZ 400 K developer (at 1:4 dilution), rinsing in DI water and drying, the sample was mounted at an angle in a deep UV flood exposure system. The angle chosen for mounting the sample is related to the final angle obtained in the PMGI layer by Snell's law for refraction at the air-PMGI interface (refractive index for PMGI ~ 1.54). The patterned AZ 5214 layer atop the PMGI sets

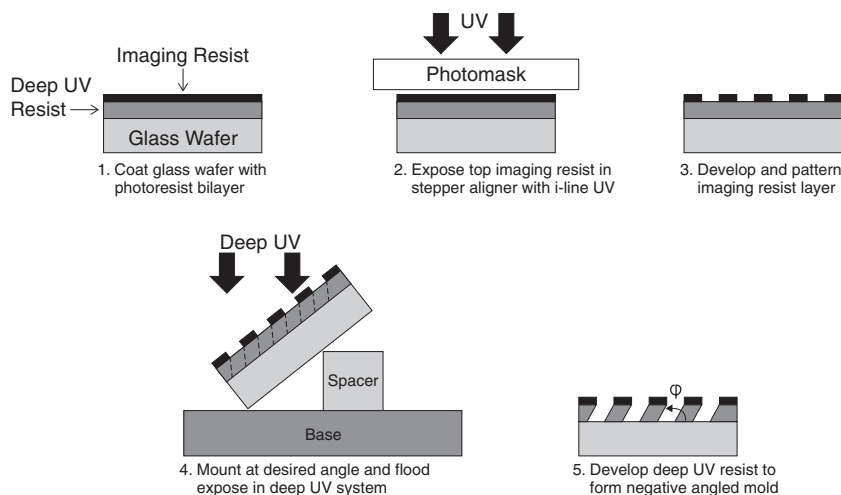


Figure 4. Schematic of the microfabrication process used to fabricate a negative mold for angled (tilted, asymmetric) PDMS microflaps. A two stage lithography process was used, the lateral features being defined by the first stage (steps 1 to 3 in the schematic), the angle ϕ being set by the second stage (steps 4 and 5). A glass wafer was used as the substrate to minimize reflections during the angled exposure step 4.

the lateral dimensions of the angled flaps by acting as a mask during the deep UV flood exposure step. Both the total exposure time (at a constant lamp power of 1000 W) and the total develop step time (in PMGI 101 developer—MicroChem Corp., Newton, MA) were tuned to increase the depth to thickness aspect ratio of the angled slots while minimizing undercut. These parameters were further improved by dividing the PMGI exposure step of 2700 seconds and the develop step of 7 min into a series of six equally long exposure and develop steps. This process enabled fabrication of angled flaps $\sim 10 \mu\text{m}$ in height ($10.8 \mu\text{m}$ measured along the tilt) and $\sim 4 \mu\text{m}$ thick, with an angle of $\sim 20^\circ$ from the vertical.

Before molding PDMS flaps using the PMGI negative molds, the durability of the molds were increased (to facilitate reuse) by hard baking the patterned PMGI resist at 110°C for 1 min. The molds were also then exposed to an oxygen plasma for 2 min, followed by deposition of a silane layer to facilitate easy peel-off. PDMS molding was then done using the same scheme described earlier for molding vertical flaps with silicon negative molds, taking care to only peel with the direction of tilt to avoid damage to the angled flaps and to the photoresist mold.

Ongoing fabrication efforts are aimed at further increasing the aspect ratio and reducing the undercut in the PMGI layer, which translates as a bulged out region in the PDMS flaps (as seen in Figure 2b).

2.2. Adhesion and Friction Testing

In order to quantify the adhesion and friction properties of the fabricated structures, a 3D displacement and force sensing probe attachment for the surface forces apparatus (SFA) 2000 was developed (Figure 5). The new attachment can generate both normal and lateral movement of surfaces, and measures the resulting normal and lateral forces independently.^[26] It was designed to let us do both load/pull and load/drag/pull tests of the fabricated structures on a small scale with a contact area of around $0.1\text{--}1 \text{ mm}^2$. The actual contact area depends on the applied load. The bottom disk is mounted in a normal load sensor in the SFA 2000. The sensor has 4 foil strain gauges (Vishay Micro-Measurements) glued symmetrically to the bending arms of the double cantilever spring, forming a

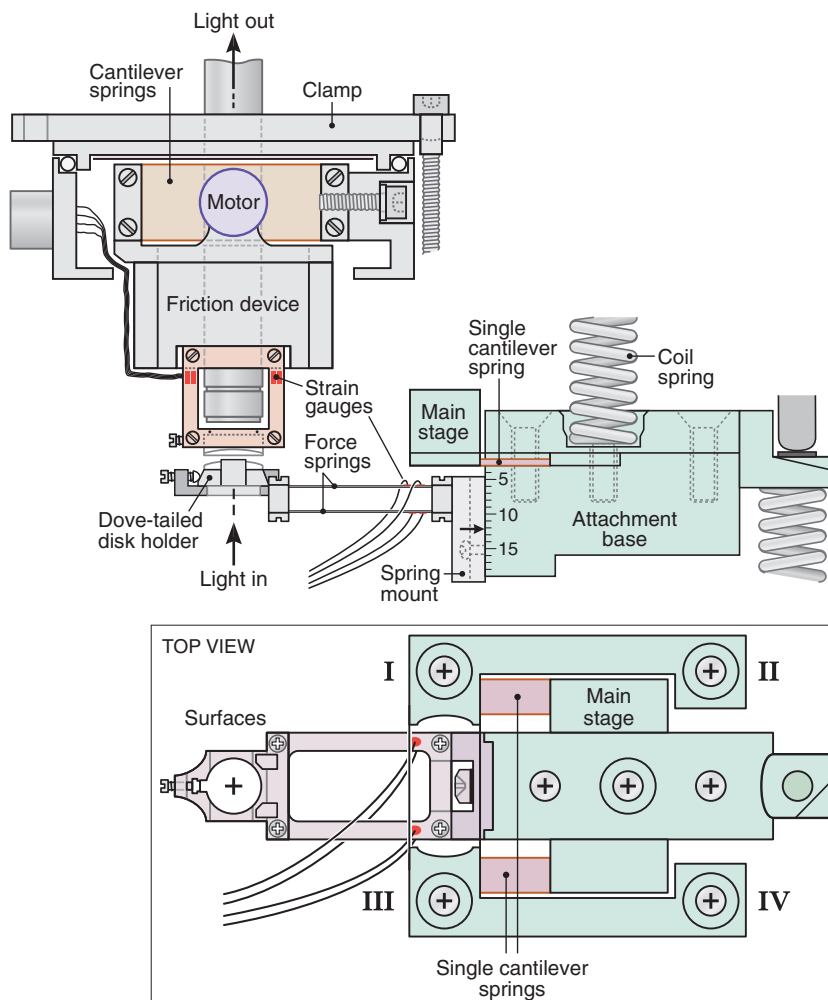


Figure 5. Schematic of the experimental set-up showing the main features of the 3D force-displacement-sensor attachment to the SFA 2000. This attachment allows 3D translation and (independent) force sensing.

Wheatstone bridge strain gauge system. When a normal force is applied to the surfaces, the strain gauges are used to measure the deflection of the spring with a signal conditioning amplifier (Vishay Measurements, 2300), which outputs the signal to either a computer data acquisition system or a chart recorder. The voltage signal is then calibrated against the weight. The top surface is held by a friction device that can move laterally with a sliding distance of between 200 and 500 μm . Driven by a reversible DC motor, the friction device can slide the upper disk back and forth smoothly with respect to the lower disk at different constant or variable speeds using a function generator. With the same force sensing mechanism as the normal load sensor, the friction device can measure the lateral shearing force (friction) during the sliding of the top surface.

The adhesion and friction tests were done with a spherical glass disk compressed/sliding against an opposing microflap/polymer substrate. Before the experiment, a thin PDMS sheet with fabricated PDMS microflaps was glued onto a flat glass disk. The disk was then mounted into the normal load sensor of a SFA box for further measurement. A spherical glass disk with a radius of 2 cm was mounted to the top friction device. Prior to use, the glass disks were soaked in chloroform (EMD Chemical Inc., Gibbstown, NJ) for 1 day and then rinsed thoroughly with ethanol followed by drying in dry nitrogen gas.

In the SFA experiment, the spherical glass disk was first pressed against the PDMS microflaps at a constant speed of about $0.06 \mu\text{m s}^{-1}$ until a desired load was reached. To measure the adhesion forces, the two surfaces were separated from each

other at an angle perpendicular to the bottom surface at the same speed. In the friction measurement, a square wave voltage function with peak to peak voltage of 20 V was applied to the dc motor to shear the upper surface at a constant velocity of $\pm 20 \mu\text{m s}^{-1}$. The spherical disk slid a distance of 200 μm forwards and backwards in the direction perpendicular to the long or short edges of the fabricated flaps. The friction test was repeated on the flaps geometry eight to ten times at the same spot. When the sliding concluded, the adhesion after sliding was measured during the separation of two surfaces.

3. Results and Discussion

3.1. Vertical Flaps

The vertical PDMS microflaps (**Figure 6a**) exhibit strong adhesion against the glass surface, as shown in **Figure 6b**. During testing the vertical pillars were compressed axially until they either buckle or are slightly bent over due to the curvature of the sphere. Upon separation, strong adhesion was evident by the rapid jump of the output voltage of the normal load sensor in the SFA setup. No adhesion was measured with a zero preload, which is due to the geometry of our experimental setup: the flaps need to deform elastically in order to make a larger contact area with the upper sphere disk, and a finite preload is therefore required. At low loads ($F_{\perp} < 5 \text{ mN}$), the adhesion force

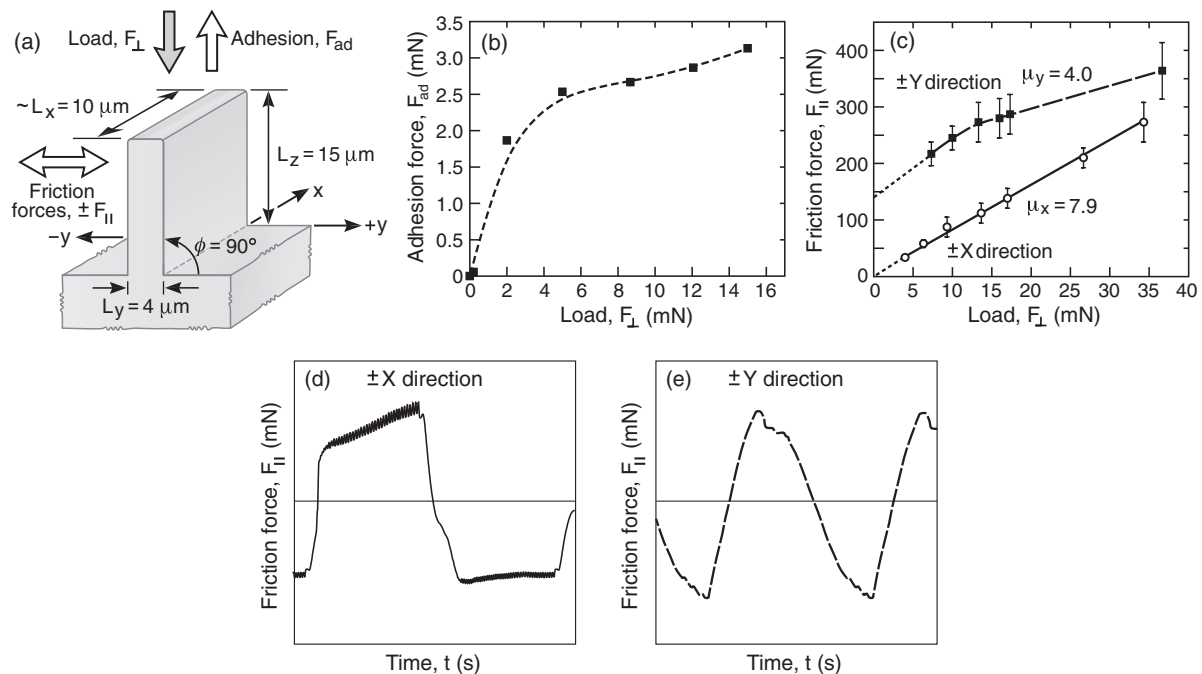


Figure 6. Adhesion forces F_{ad} , and friction forces F_{\parallel} , of the vertical (symmetric, not tilted) PDMS flaps. a) Schematic of a single vertical flap under a normal load and shear force. b) Adhesion forces, F_{ad} of the vertical flaps as a function of the preload force. c) Friction forces $\pm F_{\parallel}$, in both the $\pm x$ and $\pm y$ directions as functions of the load, F_{\perp} . The vertical flaps exhibit isotropic friction in both the $\pm x$ and $\pm y$ directions, but these are different (anisotropic) in the x - versus the y -directions. The friction is purely 'load-controlled' in the $\pm x$ directions (along the long flap edges), while in the $\pm y$ directions the friction is 'adhesion-controlled' at low loads ($F_{\perp} < 15 \text{ mN}$), becoming more load-controlled at higher loads. d) The friction trace in the x directions shows stick-slip spikes. e) No stick-slip spikes are recorded when sliding in the y directions.

increases rapidly with increasing load; the increase continues but becomes much slower at higher loads. A larger F_{\perp} gives rise to a larger elastic deformation of the PDMS flaps, resulting in a higher number of contacts as well as larger contact area of a single contact and therefore greater adhesion.

Strong anisotropic frictional behaviors were observed while sliding the upper glass disk along differently directions of the vertical flaps. Sliding in the $\pm x$ direction, perpendicular to the smaller face, shows only load-controlled friction where the friction force F_{\parallel} is directly proportional to the normal load F_{\perp} with a friction coefficient of 7.9 (Figure 6c). While sliding towards the large edge of flaps, in the $\pm y$ direction, F_{\parallel} is adhesion-controlled at loads less than 15 mN, indicated by the nonlinear relationship between F_{\parallel} and F_{\perp} . When $F_{\perp} > 15$ mN, a linear dependence of F_{\parallel} on F_{\perp} is measured with a load controlled friction coefficient of 4.0. Higher F_{\parallel} was measured when sliding along the y direction at low F_{\perp} , which also demonstrates the adhesion contribution on the friction. Since preload is required to generate adhesion, as indicated in the adhesion test, no F_{\parallel} is measured when $F_{\perp} = 0$.

Interestingly, sliding in the $\pm x$ direction also gave very regular stick-slip, Figure 6d, whereas no regular stick slip spikes were observed while sliding in the $\pm y$ direction, Figure 6e. The width of the microflaps is about 2.5 times bigger than the thickness and therefore the stiffness along the smaller face of the flaps is much higher. Our SFA results demonstrate that this anisotropic stiffness of the PDMS microflaps in different directions is crucial to both the friction and adhesion properties of the vertical flaps. For a small deflection, assuming that deformation is governed by small-deflection cantilever bending, the stiffness of a vertical flap is

$$k = \frac{3EI}{L^3} \quad (3)$$

where $E = 0.75$ MPa is the elastic modulus of the crosslinked PDMS, L is the height of the flap, and I is the area moment of inertia. I can be calculated by

$$I = \frac{bh^3}{12} \quad (4)$$

where b is the width along the bending direction and h is the thickness in the bending direction. Using the size of the vertical PDMS flaps fabricated, we can get $I_x = 0.333 \times 10^{-21} \text{ m}^4$ and $I_y = 0.053 \times 10^{-21} \text{ m}^4$. The stiffness of the vertical flaps is proportional to the area moment of inertia, $k \propto I$. A single vertical flap is therefore 6 times stiffer in the $\pm x$ direction than in the $\pm y$ direction. Due to this higher stiffness, the flaps are hard to deform elastically in the $\pm x$ direction, which causes the stick-slip spikes during sliding. This stick-slip motion could be explained by the surface topology model of stick-slip: as the sphere disk hits a new array of flaps during sliding, a resisting force is generated by the elastic deformation of flaps, causing the sticking of the glass disk.^[27] However, once the driving force overcomes the peak resisting force, the upper surface will slide down rapidly to the next array of flaps, resulting in a slip. The regular patterns give very regular stick-slip spikes in the friction trace. In the surface topology model, a stiffer material will

lead to shorter slips due to the shorter recoil to the elastic equilibrium, which allows sticking to more of the smaller asperities. Therefore, stick-slip motion is only observed during the sliding in the $\pm x$ direction, whereas no regular stick-slip is observed in the $\pm y$ direction due to the low stiffness of the flaps in that direction. The high stiffness also prevents a large contact area between the spherical glass disk and the microflaps, and therefore eliminates strong adhesion between surfaces, which would explain the pure load-controlled behavior of the friction when sliding along the $\pm x$ direction. The smaller stiffness along the large face makes the flaps easier to bend over during sliding, which gives rise to a larger contact area and thus causes the adhesion-controlled friction at low normal loads.

3.2. Angled Flaps

The angled flaps tested by the SFA are $\sim 10 \mu\text{m}$ in height and are tilted by about 20° from the vertical (Figure 7a). Highly anisotropic frictional behaviors were observed during the friction test. The friction of the flaps sliding along the $\pm x$ direction is again mainly load-controlled. F_{\parallel} is proportional to F_{\perp} with a friction coefficient of ~ 3 . The large width of the flaps gives high bending stiffness and therefore a small contact area during sliding, which limits the adhesion between the flaps and the glass disk. The SEM image also shows that the top surface of the flaps is very rough, which further eliminates the real contact area and the adhesion. On the other hand, strong adhesion-controlled friction was evident while moving the glass surface in the forward y direction, $+y$ direction. The tilted angle makes the flaps easier to bend over elastically along the $+y$ direction while sliding towards the tilted angle. This elastic deformation results in a larger contact area, therefore giving stronger adhesion. Because of the adhesion contribution to the total friction force, sliding along the $+y$ direction had higher F_{\parallel} at low F_{\perp} . However, at high F_{\perp} ($F_{\perp} > 10$ mN), the sliding friction in the x direction increases faster than in the $+y$ direction (Figure 7b). The easier bend over of the flaps in the $+y$ direction leads to a smaller resistance while sliding, resulting in a lower friction coefficient, μ_{+y} , than the friction coefficient, μ_x , in the $\pm x$ direction. At low load, although sliding along the $\pm x$ direction gives a higher friction coefficient, the load contribution is small, and the adhesion controlled friction dominates the total friction force, which results in an overall higher friction force for the $+y$ direction sliding. At high F_{\perp} , however, the load contribution wins out over the adhesion contribution, $\mu_x F_{\perp} > \mu_{+y} F_{\perp} + S_c A_{\text{real}}$, and therefore the friction force in the $\pm x$ direction is higher in this regime. The friction force in the y direction is also very anisotropic: sliding along the $+y$ direction gives a much higher friction force than sliding in the $-y$ direction (backward direction) under the same preload (Figure 7b). Similar behavior was also found in the friction test of a single gecko seta.^[13]

Unlike the vertical flaps, which showed strong adhesion after applied normal loads without sliding, the angled flaps did not show strong adhesion in the stationary adhesion test. The adhesion force was very low and never exceeded 0.1 mN for preloads between 0.8 and 6.5 mN. The small adhesion in the stationary adhesion test could be due to the effect of surface roughness. SEM images show that the top edge of the flaps is very rough.

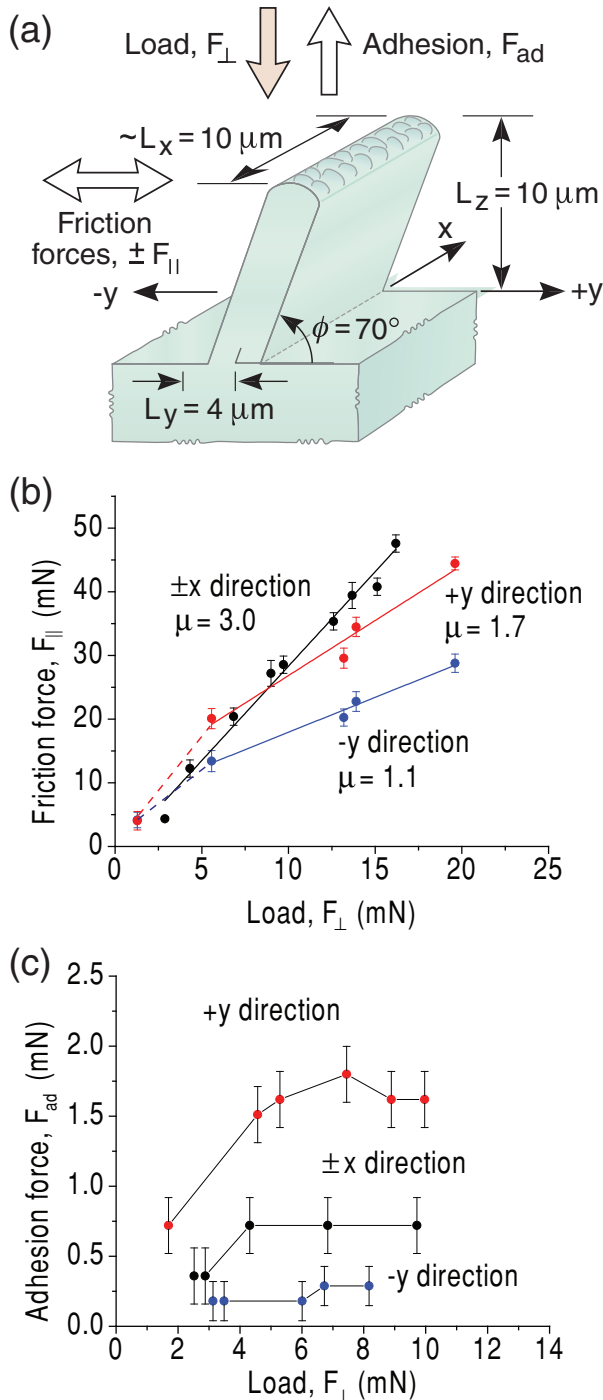


Figure 7. a) Schematic of a single angled long flap. The block arrows show the normal load and the shear force in the $\pm y$ directions as functions of the load. b) The friction forces of the angled flaps when sliding in the $\pm x$ and $\pm y$ directions. c) Sliding along the $\pm x$ directions gives almost a constant but weak adhesion regardless of the preload. In the y direction, the tilt angle strongly affects the adhesion: sliding along the $+y$ direction enhances the adhesion force, while moving in the $-y$ direction gives the lowest adhesion values, even lower than in the x direction.

Although we cannot estimate exactly the roughness of the top edge, the SEM images clearly show asperities on the order of hundreds of nanometers. This surface roughness could eliminate

the real contact area. Although the real adhesion probably slightly increases with increasing the preload, the increase is very small and cannot be measured by our current experimental setup.

Sliding of the two surfaces, meanwhile, gave much stronger adhesion forces. To test the effect of sliding, the upper glass disk was first slid back and forth for 8 cycles, and the friction force was measured during the sliding. After stopping the sliding of the upper disk, the two surfaces were separated slowly by a motor and the adhesion force was recorded. Our results show that the adhesion force depends on the sliding direction. The adhesion force measured after sliding along the $\pm x$ direction increases slightly with increasing F_\perp and then levels off at high F_\perp with a maximum adhesion of ~ 0.7 mN. There is no directional dependence while sliding in the $\pm x$ direction; stopping sliding along either the forward direction ($+x$ direction) or the backward direction ($-x$ direction) gave the same adhesion force under the same load. Since in the $\pm x$ direction the flaps are not angled, this isotropic behavior is expected. On the other hand, sliding in the $\pm y$ direction, the adhesion force exhibits strong directional dependence. Sliding in the $+y$ direction significantly enhanced the adhesion force even at low load. Sliding forward at a small load of $F_\perp = 1.7$ mN already gave an adhesion force of ~ 0.72 mN, a value that is even higher than the largest adhesion values measured at higher loads for both the cases of no sliding and of sliding along the $\pm x$ direction. Under higher loads, sliding forward resulted in even higher adhesion before the force reaches a plateau at around 1.6 mN (Figure 7d). However, only weak adhesion forces (less than 0.4 mN) were measured during the separation after sliding in the $-y$ direction, and the forces were almost a constant for the different loads tested.

The role of the tilted angle has been explained by Autumn et al.^[28] The tilted angle gives rise to an anisotropic stiffness of the flaps. The displacement of an angled flap with a tilted angle j under a normal load F_\perp and a shear force $F_{||}$ could be estimated by

$$\Delta_{\text{approx}} = \frac{L_z^3}{3EI} [F_\perp \cos^2(\varphi) \pm F_{||} \sin(\varphi) \cos(\varphi)] \quad (5)$$

The stiffness of the flaps is therefore

$$k_{\text{approx}} = \frac{F_{||}}{\Delta_{\text{approx}}} = \frac{F_{||}}{\frac{L_z^3}{3EI} [F_\perp \cos^2(\varphi) \pm F_{||} \sin(\varphi) \cos(\varphi)]} \quad (6)$$

In the above equations, take the positive sign if sheared in the direction of tilt (the $+y$ direction), and negative if sheared in the opposite direction (the $-y$ direction). This simple model predicts the anisotropic stiffness of the angled flaps: sliding against the direction of tilted direction gives higher stiffness, and sliding in the tilt direction results in lower stiffness.

This direction dependent stiffness strongly affects the adhesion properties of the flaps (Figure 8). For only the normal adhesion test without shearing, due to the top surface roughness of the flaps, the flaps only make point contacts with the glass surface. The small contact area results in small adhesion that is insensitive to preload. Our observation also agrees with previous SFA experiments on randomly rough surfaces, which demonstrated that the adhesion between a randomly rough surface

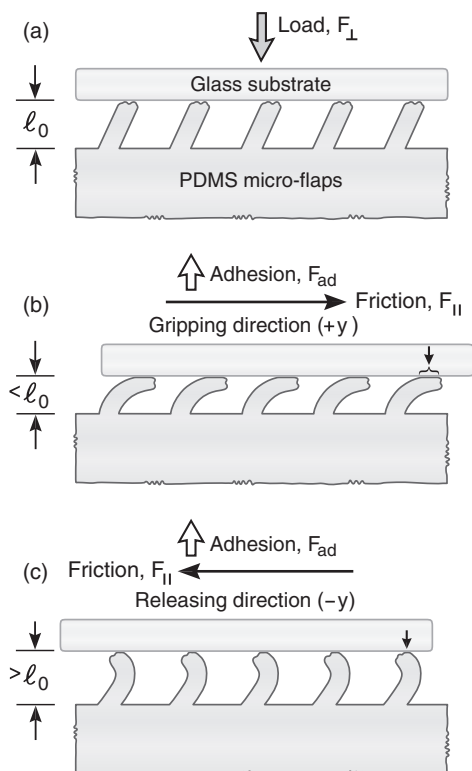


Figure 8. Schematic of the frictional adhesion mechanism of the angled flaps. a) The glass surface makes only point contact with the flaps due to the surface roughness of the flaps when only a normal load is applied. b) Sliding in the gripping direction (the +y direction) causes the flaps to bend over. The flaps are pulled towards the glass surface, giving a large contact area and high adhesion. c) Sliding in the releasing direction (the -y direction), the flaps are pulled away from the glass surface.

and a molecularly smooth bare mica surface decreased exponentially with increasing roughness and the adhesion did not increase significantly with increasing loads at high root mean square roughness (RMS).^[29,30] During testing with sliding in the +y direction, the flaps, pre-angled in the fabrication process, bend down easily as they slide over the glass surface, leading to a large contact area. This increase of contact area can give rise to both high adhesion and friction. In our SFA test, this increase of contact area was observed to lead to a two to eight fold increase of adhesion over the pure adhesion test result. At low loads, strong adhesion causes adhesion-controlled friction, which gives much higher friction forces. While sliding in the -y direction, the flaps are sheared backward. The tilted angle of the flaps prevents large bending over to the backward direction, and therefore the flaps are pulled away from the surface, leading to a smaller contact area and smaller adhesion and friction. Frictional adhesion is the unique mechanism applied by the gecko to achieve its extraordinary climbing ability. In many robotic applications, the problem is making adhesives that can rapidly detach from the surface rather than simply strongly adhering to the surface. By careful design of the geometrical and mechanical properties of the microflaps, we can apply the same mechanism to artificial dry adhesives, which could solve this problem perfectly by using the same approach as nature.

4. Conclusion

Our experimental results demonstrate how surfaces with directionally oriented or tilted structures can generate anisotropic adhesion and friction when articulated in a specific manner, thus, the tilted micro flaps give rise to both strong friction and adhesion forces when sliding along the tilted direction, and low friction and adhesion forces when sliding against the tilted direction. This appears to be the method employed by geckos allowing them to run on the (vertical) walls and (horizontal) ceilings: the anisotropic, directionally tilted flaps provide simultaneous strong adhesion and friction for attachment (in the gripping stage) and weak adhesion and friction for detachment (in the releasing stage) during a step cycle. The anisotropy built into the design allows for controllability and switchability by varying the flap dimensions, density, tilt angle, and shearing direction. These results may be the first step to generate a quantitative scaling model for fabricating gecko-mimetic feet structures for designing responsive adhesives and climbing robotics applications.

Acknowledgements

This work was sponsored by the Institute for Collaborative Biotechnologies Grant No. DAAD19-03-D-0004 from the U.S. Army Research Office, and by National Science Foundation NIRT Grant No. 0708367. Part of this work was done in the UCSB nanofabrication facility, part of the NSF-funded National Nanotechnology Infrastructure Network (NNIN). Jing Yu and Sathya Chary contributed equally to this work.

Received: March 3, 2011

Revised: May 5, 2011

Published online:

- [1] R. Ruibal, V. Ernst, *J. Morphol.* **1965**, *117*, 271.
- [2] K. Autumn, M. Sitti, Y. C. A. Liang, A. M. Peattie, W. R. Hansen, S. Sponberg, T. W. Kenny, R. Fearing, J. N. Israelachvili, R. J. Full, *Proc. Natl. Acad. Sci. USA* **2002**, *99*, 12252.
- [3] G. Huber, H. Mantz, R. Spolenak, K. Mecke, K. Jacobs, S. N. Gorb, E. Arzt, *Proc. Natl. Acad. Sci. USA* **2005**, *102*, 16293.
- [4] N. S. Pesika, H. B. Zeng, K. Kristiansen, B. X. Zhao, Y. Tian, K. Autumn, J. Israelachvili, *J. Phys-Condens. Mat.* **2009**, *21*.
- [5] D. J. Irschick, C. C. Austin, K. Petren, R. N. Fisher, J. B. Losos, O. Ellers, *Biol. J. Linn. Soc.* **1996**, *59*, 21.
- [6] K. Autumn, Y. A. Liang, S. T. Hsieh, W. Zesch, W. P. Chan, T. W. Kenny, R. Fearing, R. J. Full, *Nature* **2000**, *405*, 681.
- [7] N. S. Pesika, N. Gravish, M. Wilkinson, B. X. Zhao, H. B. Zeng, Y. Tian, J. Israelachvili, K. Autumn, *J. Adhesion* **2009**, *85*, 512.
- [8] B. N. J. Persson, *J. Chem. Phys.* **2003**, *118*, 7614.
- [9] B. N. J. Persson, S. Gorb, *J. Chem. Phys.* **2003**, *119*, 11437.
- [10] H. B. Zeng, N. Pesika, Y. Tian, B. X. Zhao, Y. F. Chen, M. Tirrell, K. L. Turner, J. N. Israelachvili, *Langmuir* **2009**, *25*, 7486.
- [11] N. S. Pesika, Y. Tian, B. X. Zhao, K. Rosenberg, H. B. Zeng, P. McGuiggan, K. Autumn, J. N. Israelachvili, *J. Adhesion* **2007**, *83*, 383.
- [12] Y. Tian, N. Pesika, H. B. Zeng, K. Rosenberg, B. X. Zhao, P. McGuiggan, K. Autumn, J. Israelachvili, *Proc. Natl. Acad. Sci. USA* **2006**, *103*, 19320.
- [13] B. X. Zhao, N. Pesika, K. Rosenberg, Y. Tian, H. B. Zeng, P. McGuiggan, K. Autumn, J. Israelachvili, *Langmuir* **2008**, *24*, 1517.
- [14] B. X. Zhao, N. Pesika, H. B. Zeng, Z. S. Wei, Y. F. Chen, K. Autumn, K. Turner, J. Israelachvili, *J. Phys. Chem. B* **2009**, *113*, 3615.

- [15] A. K. Geim, S. V. Dubonos, I. V. Grigorieva, K. S. Novoselov, A. A. Zhukov, S. Y. Shapoval, *Nat. Mater.* **2003**, *2*, 461.
- [16] S. Gorb, M. Varenberg, A. Peressadko, J. Tuma, *J. R. Soc. Interface* **2007**, *4*, 271.
- [17] M. T. Norten, C. Greiner, E. Arzt, K. L. Turner, *Adv. Mater.* **2008**, *20*, 3905.
- [18] D. Sameoto, C. Menon, *J. Micromech. Microeng.* **2009**, *19*.
- [19] C. Greiner, E. Arzt, A. del Campo, *Adv. Mater.* **2009**, *21*, 479.
- [20] B. Aksak, M. P. Murphy, M. Sitti, *Langmuir* **2007**, *23*, 3322.
- [21] J. Lee, C. Majidi, B. Schubert, R. S. Fearing, *J. R. Soc. Interface* **2008**, *5*, 835.
- [22] H. E. Jeong, J. K. Lee, H. N. Kim, S. H. Moon, K. Y. Suh, *Proc. Natl. Acad. Sci. U. S. A.* **2009**, *106*, 5639.
- [23] T. I. Kim, H. E. Jeong, K. Y. Suh, H. H. Lee, *Adv. Mater.* **2009**, *21*, 2276.
- [24] E. Arzt, S. Gorb, R. Spolenak, *Proc. Natl. Acad. Sci. U. S. A.* **2003**, *100*, 10603.
- [25] A. Peressadko, S. N. Gorb, *J. Adhesion* **2004**, *80*, 247.
- [26] J. Israelachvili, Y. Min, M. Akbulut, A. Alig, G. Carver, W. Greene, K. Kristiansen, E. Meyer, N. Pesika, K. Rosenberg, H. Zeng, *Rep. Prog. Phys.* **2010**, *73*.
- [27] A. D. Berman, W. A. Ducker, J. N. Israelachvili, *Langmuir* **1996**, *12*, 4559.
- [28] K. Autumn, C. Majidi, R. E. Groff, A. Dittmore, R. Fearing, *J. Exp. Biol.* **2006**, *209*, 3558.
- [29] M. Benz, K. J. Rosenberg, E. J. Kramer, J. N. Israelachvili, *J. Phys. Chem. B* **2006**, *110*, 11884.
- [30] B. Zappone, K. J. Rosenberg, J. Israelachvili, *Tribol. Lett.* **2007**, *26*, 191.